The Excited Hydrogen Atom in Parallel Electric and Magnetic Fields

A thesis submitted in partial fulfillment of the requirements for the degree of Bachelor of Science with Honors in Physics from the College of William and Mary in Virginia

by
Abigail Acton Flower

Accepted for _____

_____
Advisor: Dr. John B. Delos

_____

_____

Table of Contents

Acknowledgements

I would like to thank Dr. John Delos for the tremendous amount of time, enthusiasm, and support he has given me. I feel privileged having had the experience of working under his guidance; he has a true gift for teaching. I also wish to extend my thanks to Dong Mei Wang, who has made me feel so welcome and was of invaluable help throughout the length of my research. In addition, many thanks to Vladimir Kondratovich for his support and computer help. Finally, I wish to thank the other members of my honors committee, Professor Jesse Bohl, Dr. Marc Sher, and Dr. Gina Hoatson for their time and interest.

Abstract

An excited Hydrogen atom in parallel electric and magnetic fields is studied as an example of a nonlinear system. Ultimately, the escape times of various electron trajectories in the system are studied, and a fractal relationship between escape time and initial motion is investigated, a relationship which has been found in other nonlinear systems. Expecting to find this fractal structure in the region of the heteroclinic tangle, the tangle was located and an image of it generated. It is shown that this heteroclinic tangle organizes the system's behavior in phase space.

I. Introduction

A. The system

The system is an electron in a classical orbit about a proton in the presence of parallel electric and magnetic fields[3]. Several aspects of the system invite study. First, the system is nonlinear; we can learn about nonlinear dynamics and chaos as it manifests itself in this particular situation. In this sense, I am approaching the Hydrogen atom as a means of understanding nonlinear systems. Furthermore, studying an atomic system has its own unique interest. Experimental measurements of energies and lifetimes of states can be made, and it has been shown that nonlinear dynamics manifests itself in the behavior of the atom[1,2]. In addition, studying such an atomic system allows us to look at the connection between classical and quantum behavior in chaotic systems. I am approaching the problem classically, but there is the potential for it to be treated quantum mechanically and compare the results.

I will identify the parameters of special interest to this system, identify the relevant short periodic orbits, compute the heteroclinic tangle (see section ID) of the system under these conditions, and begin to study the "lifetimes" of certain electron trajectories; in other words, to determine how long it takes an electron to escape the system (ionization). We predict, based on previous research involving similar systems, that these escape times will be closely related to other aspects of the dynamics of the system. The electron in the system has three forces acting on it: the Coulomb force with the proton it orbits, and the forces created by the static electric and magnetic fields. The Hamiltonian of the system is given by:

$$H = \frac{(\mathbf{p} - q\mathbf{A})^2}{2m_e} + qV_{total} \qquad \text{Eq. 1.1}$$

where **p** is the momentum, **A** the vector potential. The total potential is

$$V_{total} = V_{Coulomb} + V_{electric},$$

and

and

$q = -e$, the electronic charge

B. Background

It has been well substantiated that, in dissipative nonlinear systems, chaotic dynamics leads to the existence of fractal basin boundaries in phase space, that is a fractal dependence of final position on initial position[1,2,4]. Such fractal behavior can also arise in conservative systems. This fractal relation is of practical significance as it indicates that the behavior of a particle has an extremely sensitive dependence on its initial conditions.

For an inelastic collision of a helium atom with an iodine molecule, a nonlinear system studied by Jaffe and Tiyapan, it was demonstrated that a homoclinic tangle partitions the classical phase space into an invariant fractal tiling. (See section D for details on the homoclinic tangle). The tangle, in other words, organizes the phase space dynamics of the system.

I will demonstrate that similar behavior occurs in my system. It will be shown that, for short times, the escape time as a function of initial momentum is function that looks like it may be fractal. We are continuing to study the relationship between this fractal function and the tendrils of the heteroclinic tangle. Ultimately, this is a search for some sort of pattern or order to the chaos in the system.

C. Surfaces of section and their properties

When studying a nonlinear system, it is most convenient to study the dynamics in phase space. When dealing with systems of two coordinates, $(\hat{u},\hat{v})$, one then has to consider four-dimensional phase space, $(\hat{u},\hat{v},\hat{p}_u,\hat{p}_v)$. To make things comprehensible, surfaces of section are used. This involves using two of the four phase space dimensions to "strobe" the motion in the other two dimensions. For instance, every time a trajectory passes through $\hat{u}=0$ in the positive $\hat{p}_u$ sense, a point is plotted on the $\hat{v}$- $\hat{p}_v$ plane. The resulting graph is called the surface of section. This process can be thought of as a repeated mapping of an initial ($\hat{v}$, $\hat{p}_v$) point, the mapping determined by the numerically integrated Hamiltonian equations of motion.

Points generated this way may lie upon smooth curves topologically equivalent to ellipses or hyperbolas, or they may

Trajectories displaying regular motion, that is periodic or quasi-periodic, appear as concentric ellipses about a fixed stable point, called an "O-point."[5] This is illustrated in Figure 1.1.

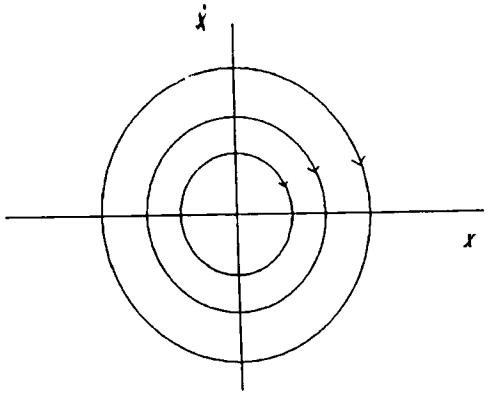

Figure 1.1. Regular motion on a surface of section appears as ellipses.[5]

This O-point is a point of stable equilibrium, and the ellipses surrounding it represent trajectories that oscillate about this fixed point, much like small angle oscillations in a pendulum.

On the other hand, trajectories representing chaotic motion appear as random scatterings of points on the surface of section. This behavior occurs in the region near unstable fixed points, called "X-points," on the surface of section, due to the occurrence of homoclinic or heteroclinic tangles. (See section D). In the case of the pendulum, these X-points represent the pendulum suspended in the inverted position, 180 degrees from equilibrium.

There are several properties of the motion in phase space that must be noted to better understand and interpret these

surfaces of section. First, since energy is conserved, the

curve that crosses a stable manifold maps to another section of a curve, also crossing the stable manifold in the same sense. Therefore, if the stable and unstable manifolds cross once, they must cross an infinite number of times.

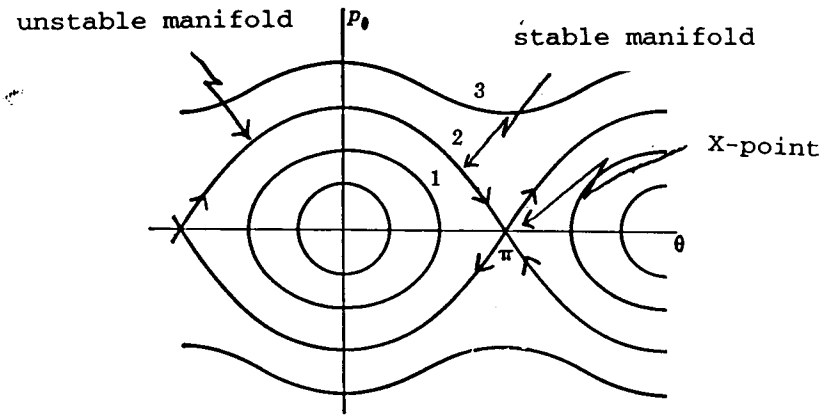

Figure 1.2. Motion of a pendulum as it appears in phase space

As the crossing points approach the X-point, they get closer and closer together. But the area enclosed between stable and unstable manifolds must be preserved. As its width decreases, its length must increase. This behavior leads to a heteroclinic or homoclinic tangle--heteroclinic, if the manifolds belong to different X-points, homoclinic if they belong to the same X-point. A heteroclinic tangle can be seen in Figure 1.3.

The heteroclinic and homoclinic orbits are asymptotic, in both the past and the future, to the unstable periodic orbits. These orbits are significant in that the bound and unbound dynamics of the system must somehow weave themselves around these orbits. The heteroclinic tangle, in this way, acts as the partition of phase space.

Often, it is such tangles that separate qualitatively different motions, similar to the pendulum case in which the manifolds separate small oscillations from rotation.

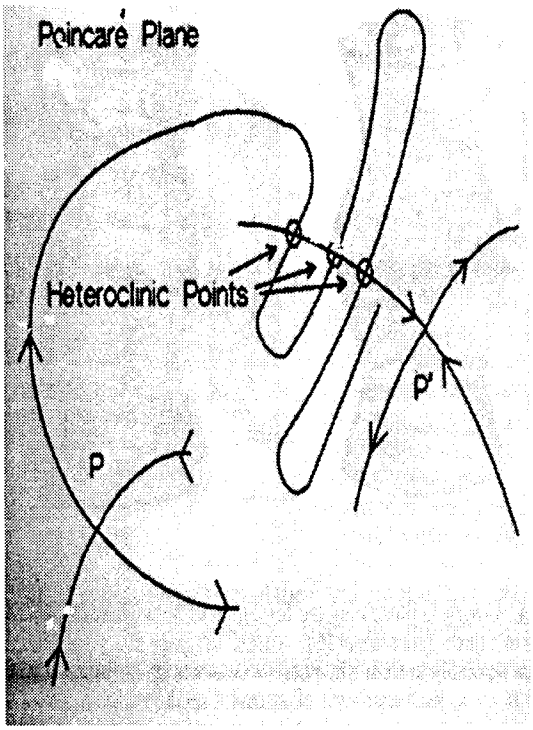

Figure 1.3. A heteroclinic tangle formed by the unstable manifold of P and the stable manifold of P', intertwining in such a way as described in text. The progressively longer "lobes" formed between consecutive heteroclinic points are called tendrils. The heteroclinic points approach P' asymptotically.

II. Orbits and Surfaces of Section

A. Transforming the Hamiltonian

It is helpful to transform the Hamiltonian (as given in equation 1.1) to a convenient set of coordinates to simplify the study of it. In order to do this, we first took advantage of the cylindrical symmetry of the system, allowing me to reduce it from a three-dimensional to a two-dimensional problem. We then, performed a series of canonical transformations on the Hamiltonian to preserve the form of the Hamiltonian equations of motion. We arrived at a Hamiltonian expressed in semi-parabolic coordinates, $(\hat{u},\hat{v})$, with a discontinuity at the origin. To alleviate this problem, it was necessary to transform to a new "time" variable. Finally, we expressed the function in atomic units and rescaled so as to remove the electric field as an explicit parameter of the system. The resulting Hamiltonian is (see Appendix A for the derivation):

$$\hat{H} = \frac{\left(\hat{p}_u^{\,2} + \hat{p}_v^{\,2}\right)}{2} - \hat{E}\left(\hat{u}^2 + \hat{v}^2\right) + \frac{\hat{B}^2}{8c^2}\left(\hat{u}^4\hat{v}^2 + \hat{u}^2\hat{v}^4\right) + \frac{\left(\hat{u}^4 - \hat{v}^4\right)}{2} - 2 \qquad \text{Eq. 2.1}$$

The rescaled energy, E, and rescaled magnetic field, B, are related to their original values and the electric field, F, by:

$$E = \hat{E}F^{\frac{1}{2}}$$

$$B = \hat{B}F^{\frac{3}{4}}$$

Conveniently, this Hamiltonian, in the absence of the third term, ($\hat{B}$= 0), is separable, and represents a 2-dimensional anharmonic oscillator with a stable equilibrium and two unstable equilibria. The contours of the potential for this separable system are shown in Figure 2.1 in semi-parabolic coordinates.

The third term in equation 2.1 is the coupling term, the term which essentially adds the element of chaos to our system, with the parameter, $\hat{B}$, determining the magnitude of its contribution to the system.

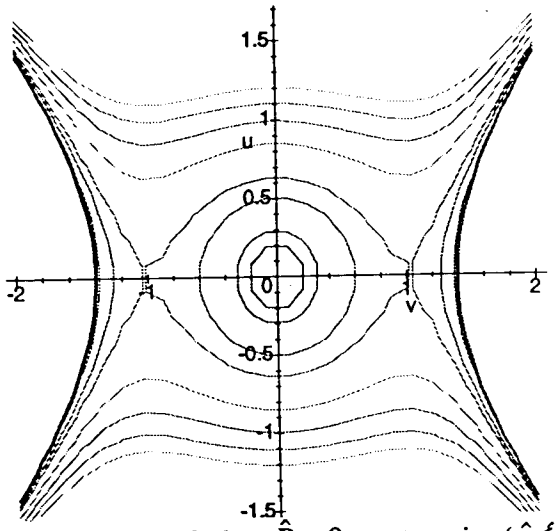

Figure 2.1. The potential of the $\hat{B}=0$ system in $(\hat{u},\hat{v})$ coordinates.

B. Creating surfaces of section

As I've already stated that the system is nonlinear, it is no surprise that the equations of motion yielded by our final Hamiltonian cannot be solved analytically; this is a characteristic of a nonlinear system. In order to study the motion of the electron, it was, therefore necessary for me to concoct a computer program to numerically integrate the equations of motion. We can calculate numerically a surface of section by the method described earlier in section IC; every time the electron passes through $\hat{u}= 0$ in the positive direction ($\hat{p}_u> 0$), a point is plotted in the $\hat{v}-\hat{p}_v$ plane. What I did instead, however, was to create a half-map, a surface of section on which a point is plotted every time $\hat{u}= 0$, regardless of the direction of $\hat{p}_u$. Such a mapping is permissible due to the special symmetry of my system. I was able to show that there exists a half-map such that, regardless of whether I map some initial point, $(\hat{v}_0,\hat{p}_{v0})$, in the positive $\hat{p}_u$ sense or the negative $\hat{p}_u$ sense, $(\hat{v}_0,\hat{p}_{v0})$ will map to the same point, $(\hat{v}_1,\hat{p}_{v1})$.

With the rescaled magnetic field parameter set equal to zero, $\hat{B}$ = 0, Figure 2.2 shows a series of concentric ellipses about a stable point located at the origin, each ellipse representing a single trajectory. Such ellipses are the mark of regular motion. This correlation comes from Liouville's Theorem, which states that for

a system in four-dimensional phase space with as many conservation laws as degrees of freedom, the motion is restricted to a two-dimensional surface topologically equivalent to a torus. With $\hat{B} = 0$, equation 2.1 meets this criterion; since the equation is separable, the effective energies associated with the $\hat{u}$ and $\hat{v}$ motion are independently conserved. When we look at Figure 2.2, we see the cross sections of the tori. Like two-dimensional motion of a harmonic oscillator, the motion has two independent frequencies.

In each successive graph, figures 2.3 to 2.5, the value of $\hat{B}$ is increased, and we can observe an increase in the amount of chaos in the system. Finally, at the rescaled magnetic field parameter, $\hat{B}$ = 90, in Figure 2.5, we see total chaos uniformly distributed over the entire system, as characterized by the seeming randomness of the scattered points.

Looking more closely at the graphs gives us some further insight into the system. In Figure 2.3, for example, we see two stable points with regular trajectories about them. There seems to be a clear boundary separating these regions of order from the large "sea" of chaos. In addition, one sees the formation of island chains. When a separable system is perturbed by a nonseparable coupling, tori with irrational frequency ratios are distorted by the coupling, but not destroyed. Tori with rational frequency ratios are destroyed, and replaced by stable and unstable periodic orbits. The stable orbits are surrounded by little islands of stability, while the unstable ones are surrounded by heteroclinic tangles, which show up on the surface of section as small regions of chaos in the phase space.

After experimenting with several parameter values, I arrived at a set of values, $\hat{E}$ = -1.9, B=6T, and F=800 V/cm ($\hat{B}$=3.26), which yielded a particularly interesting surface of section, in which approximately equal amounts of chaos and order are manifested. This surface of section was created by iterating one hundred trajectories seventy-five times. That is to say, each of the one hundred trajectories represented, passed through $\hat{u}$=0 seventy-five times.

Immediately apparent in this graph are two stable (O) points and one X-point at the origin of the graph. The presence of the large region of chaos surrounding the ellipses of order suggests the presence of a heteroclinic tangle in that area, which consequently indicates the existence of more unstable points.

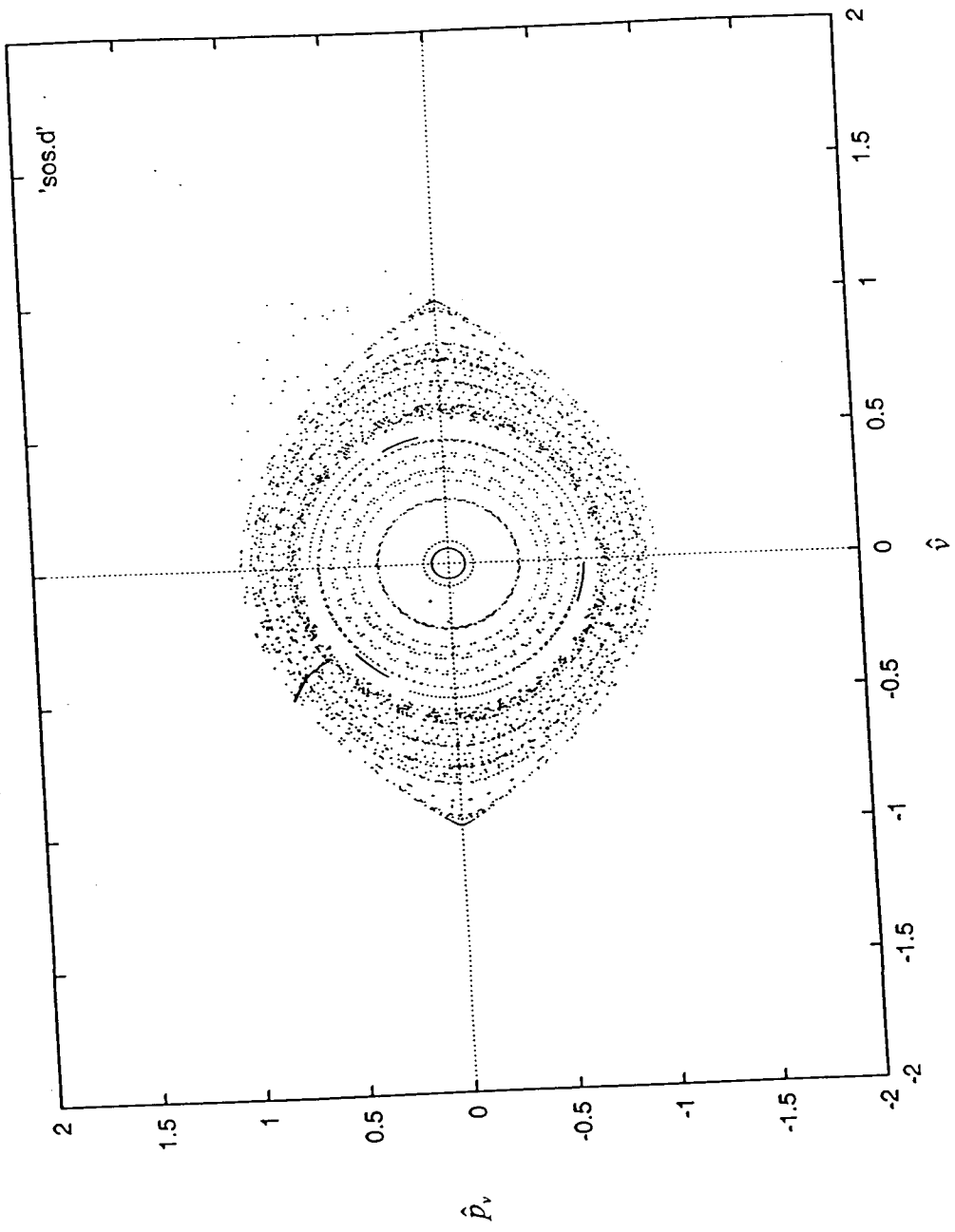

Figure 2.2. Regular motion resulting from setting $\hat{B}=0, \hat{E}=-1$. This graph represents 100 trajectories iterated 100 times.

Figure 2.3. While still primarily regular motion, as in Figure 2.1, one can see a hint of chaotic behavior surrounding the regular motion trajectories as $\hat{B}$ is now increased to 2.75.

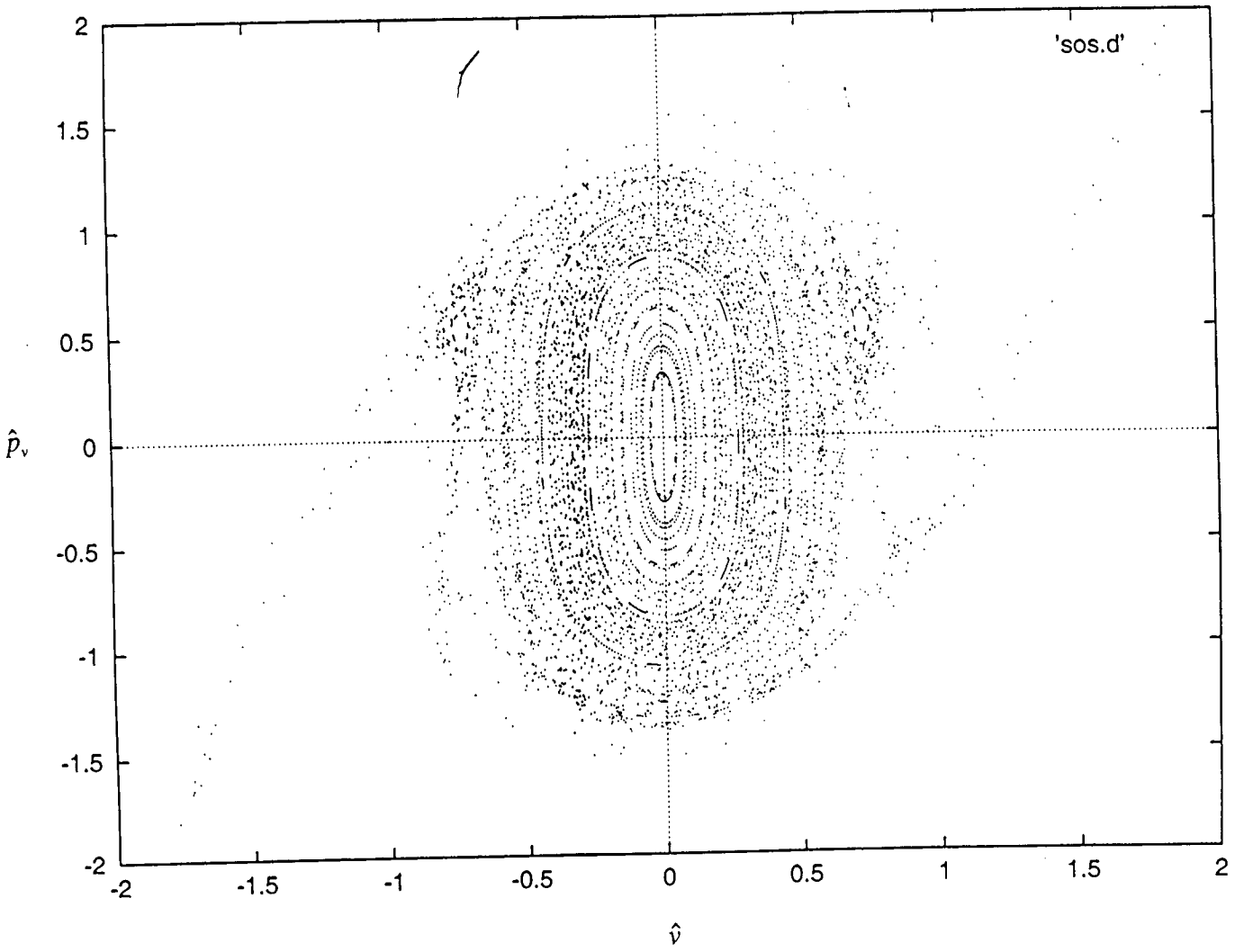

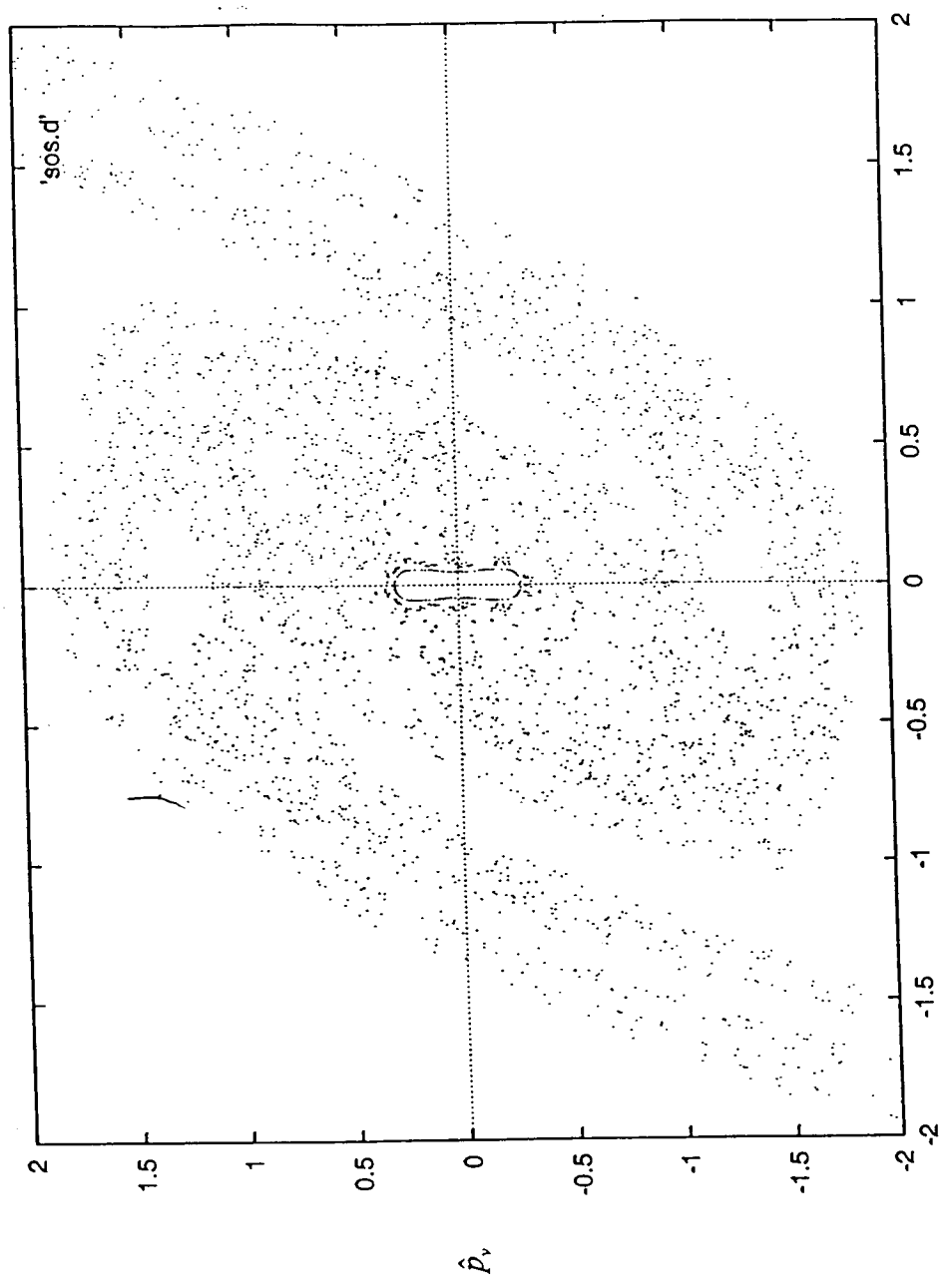

Figure 2.4. The motion is now primarily chaotic with three small regions of regular motion present. $\hat{B} = 10.5$.

Figure 2.5. The motion is completely chaotic with $\hat{B} = 60$.

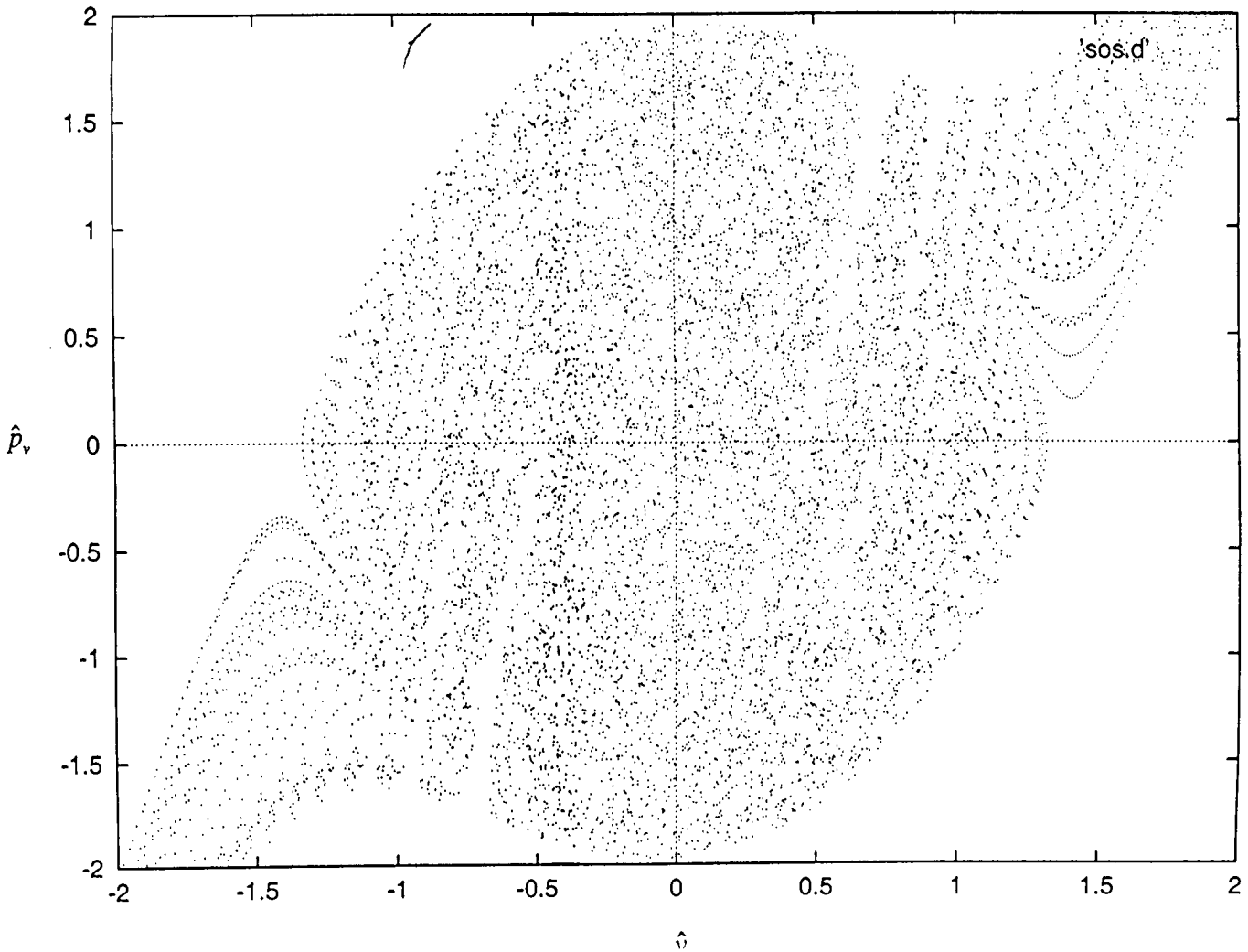

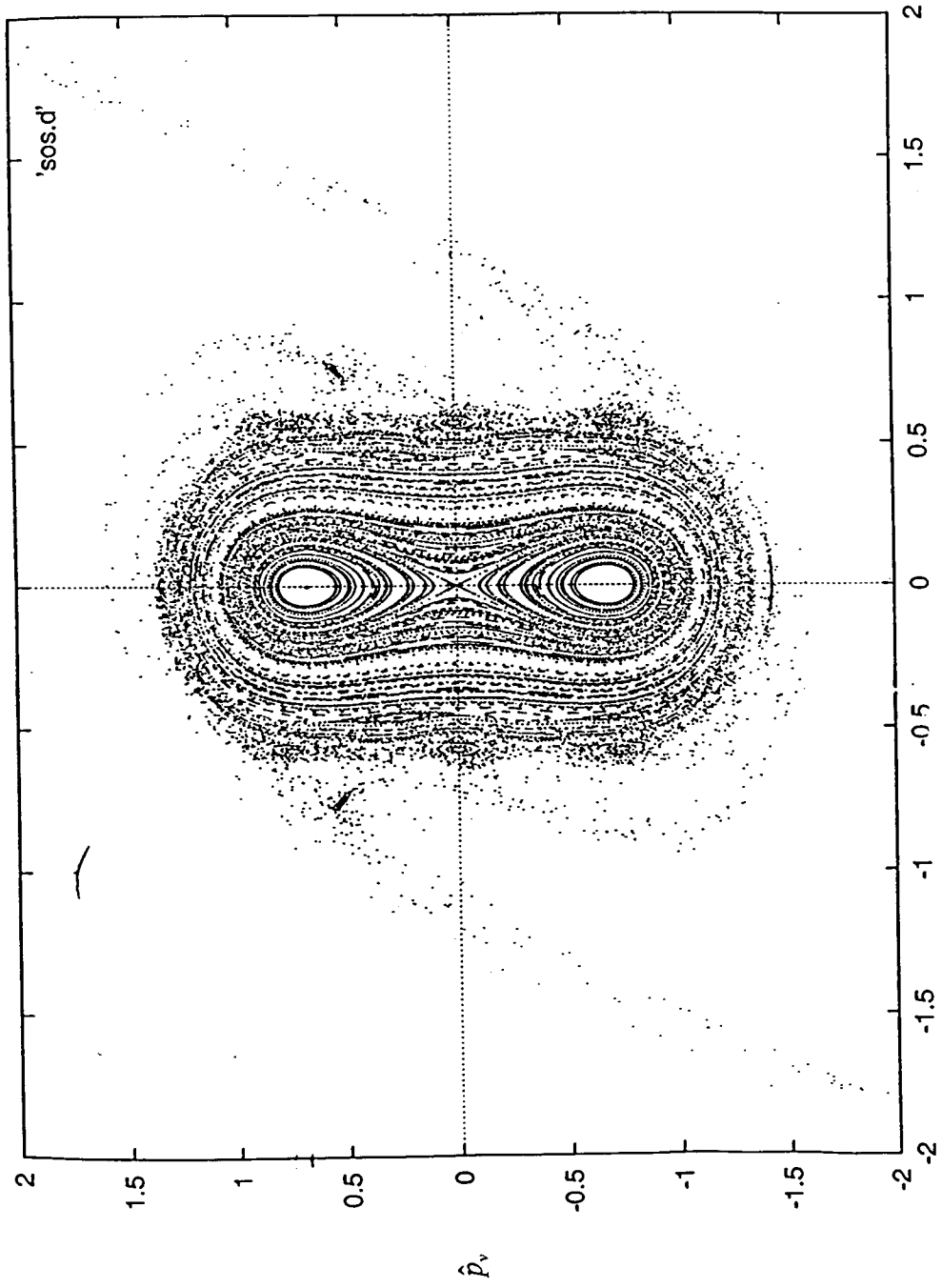

Figure 2.6. The system with $\hat{B} = 3.26, \hat{E} = -1$.

C. Locating the heteroclinic tangle

We already stated that the heteroclinic tangle "organizes" the behavior of orbits. Therefore, we need to compute this tangle. To locate it, it is first necessary to find all short periodic orbits, orbits which pass through the same point on the surface of section with every pass through $\hat{u}$=0. Now I take a grid of one thousand evenly spaced points of initial $\hat{v}$ and $\hat{p}_v$ values between -2 and 2 on the $\hat{v}$- $\hat{p}_v$ plane and iterate them once. The limits, -2 and 2, were chosen as these appear, from the surfaces of sections shown in figures 2.2 through 2.6, to be the approximate maximum radius of trajectories before they escape the system. Then I graph the contours of $\hat{v}_1 - \hat{v}_0$ and the contours of $\hat{p}_{v_1} - \hat{p}_{v_0}$. Superimposing these two graphs, wherever the zero-valued contours of each graph intersect a short periodic orbit occurs. In addition to the one at the origin, two such orbits were found, symmetric about the $\hat{p}_v$ axis located approximately at =0, $\hat{v}$=1.3 and -1.3. To identify these points to a greater degree of accuracy, I performed a single iteration of 1000 points surrounding each periodic orbit on the $\hat{v}$ axis, and thereby identified the location of the periodic orbit with higher accuracy. I repeated this process with progressively smaller intervals until I was able to locate the fixed points to eight significant figures at $\hat{v}$=1.278915389 and $\hat{v}$=-1.278915389.

Taking advantage of the symmetry of these points, I focused my attention only on the periodic orbit of the positive v-axis. While 8-significant figure precision accurately discloses the location of the X-point for my purposes, it is not exact; when this point is iterated multiple times, it eventually wanders from its initial location and faintly traces the beginnings of the heteroclinic tangle, finally escaping to infinity along the unstable manifold of the X-point to which it was initially so close. This gives us a set of points on the unstable manifold. Taking a series of 1000 evenly spaced points between our X-point and a point on the unstable manifold and iterating this line of points multiple times, I was able to generate an image of the heteroclinic tangle as shown in Figure 2.7. It is this complicated structure which organizes the motion of the system near the unstable periodic orbits. (See section IID).

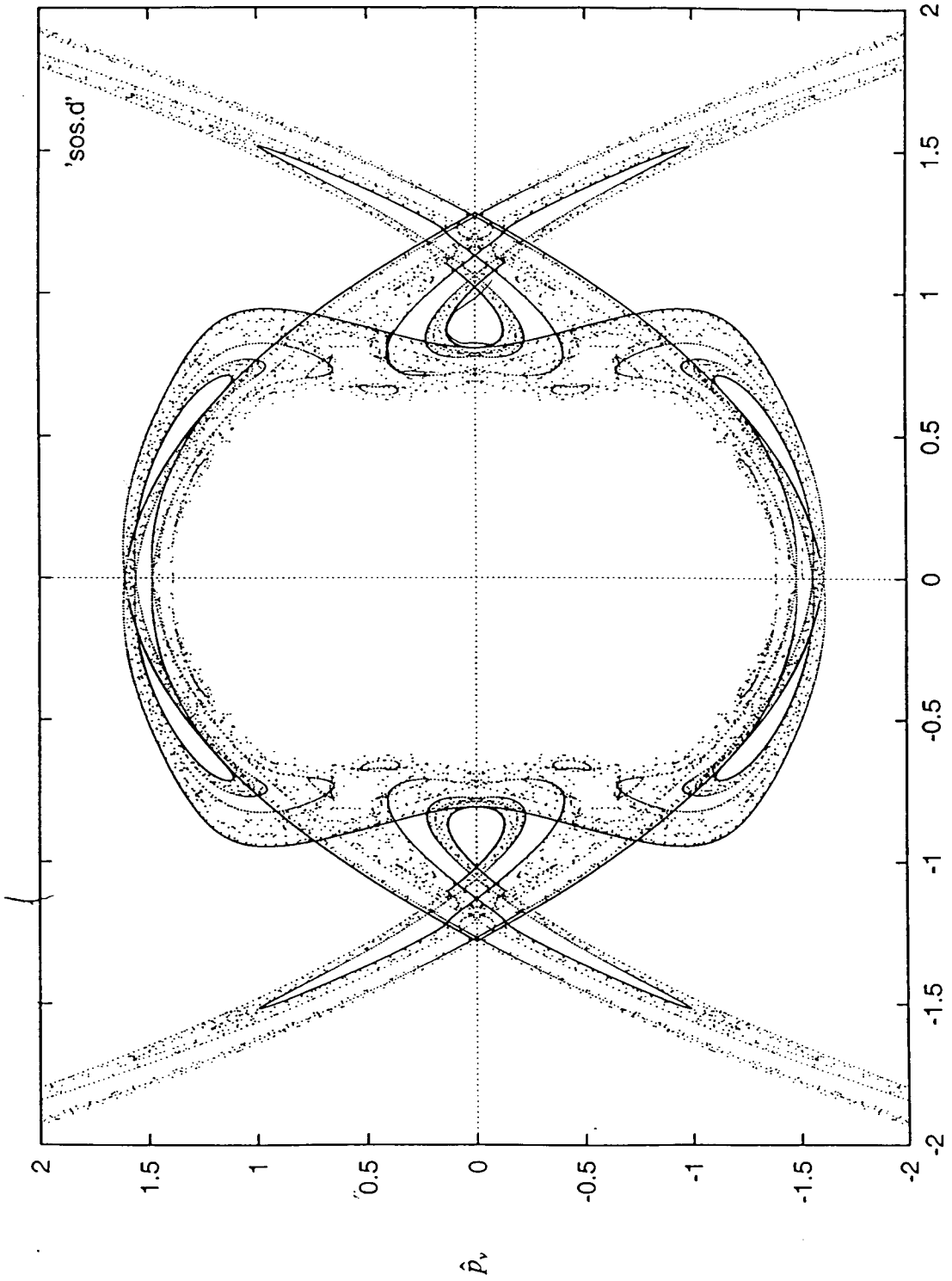

Figure 2.7. The heteroclinic tangle for this system.

III. Escape time of orbits

Now we wish to start the orbits at the origin, the location of the atom ($\hat{u}$=0, $\hat{v}$=0). We are interested in the ionization of the atom by a laser, so of course the electrons begin their travels at the atom. We, therefore, start a line of points on the $\hat{p}_v$ axis and iterate them. In the regular region of the surface of section, electrons remain forever bound to the atom and their motion is multiply periodic. When a line segment on the $\hat{p}_v$ axis corresponding to this region is iterated, the line produces a whorl. M.V. Berry explains the occurrence of such a structure as the passing of an initial curve, in our case, the line segment on the $\hat{p}_v$ axis, through a fixed elliptic point.[1] When the line segment, l_0, is iterated, l_n, the curve produced after n iterations, is pinned at this fixed elliptic point but is otherwise free to evolve. Points near the elliptic fixed point rotate around it, and the rotation rate decreases with distance. That is to say that the rate of rotation depends on the radius; it is slower at larger radii.

To get a sense of the actual motion in this region of the phase space, I generated a graph of several orbits in the region as they appear in $(\hat{u},\hat{v})$ space. In the densely covered "figure-8" region of figure 3.1, a typical orbit appears like Figure 3.2. Outside of this region, where the trajectories are less densely scattered, a typical orbit appears as Figure 3.3.

For large $\hat{p}_v$ values, the corresponding trajectories exit the system promptly along the unstable manifold. This can be verified by the mapping of a line segment corresponding to these large values, shown in Figure 3.4.

As indicated by Figure 3.5, the behavior of trajectories with $\hat{p}_v$ values started in the region of the tangle is complicated; these trajectories demonstrate the chaos caused by the tangle. If one looks carefully, one can see that the trajectories started in this region tend to map along, or close to, the heteroclinic tangle.

Further study is, therefore, to be focused on this region of the surface of section, attempting to discover an underlying pattern to the seemingly random behavior. I will concentrate my study on the trajectories that escape in a relatively short amount of time (within 8 nanoseconds).

Selecting $|\hat{v}|>2$ as my condition for escape, I began 1000 trajectories in the region of the heteroclinic tangle along the $\hat{p}_v$ axis and plotted the time of escape of these trajectories versus

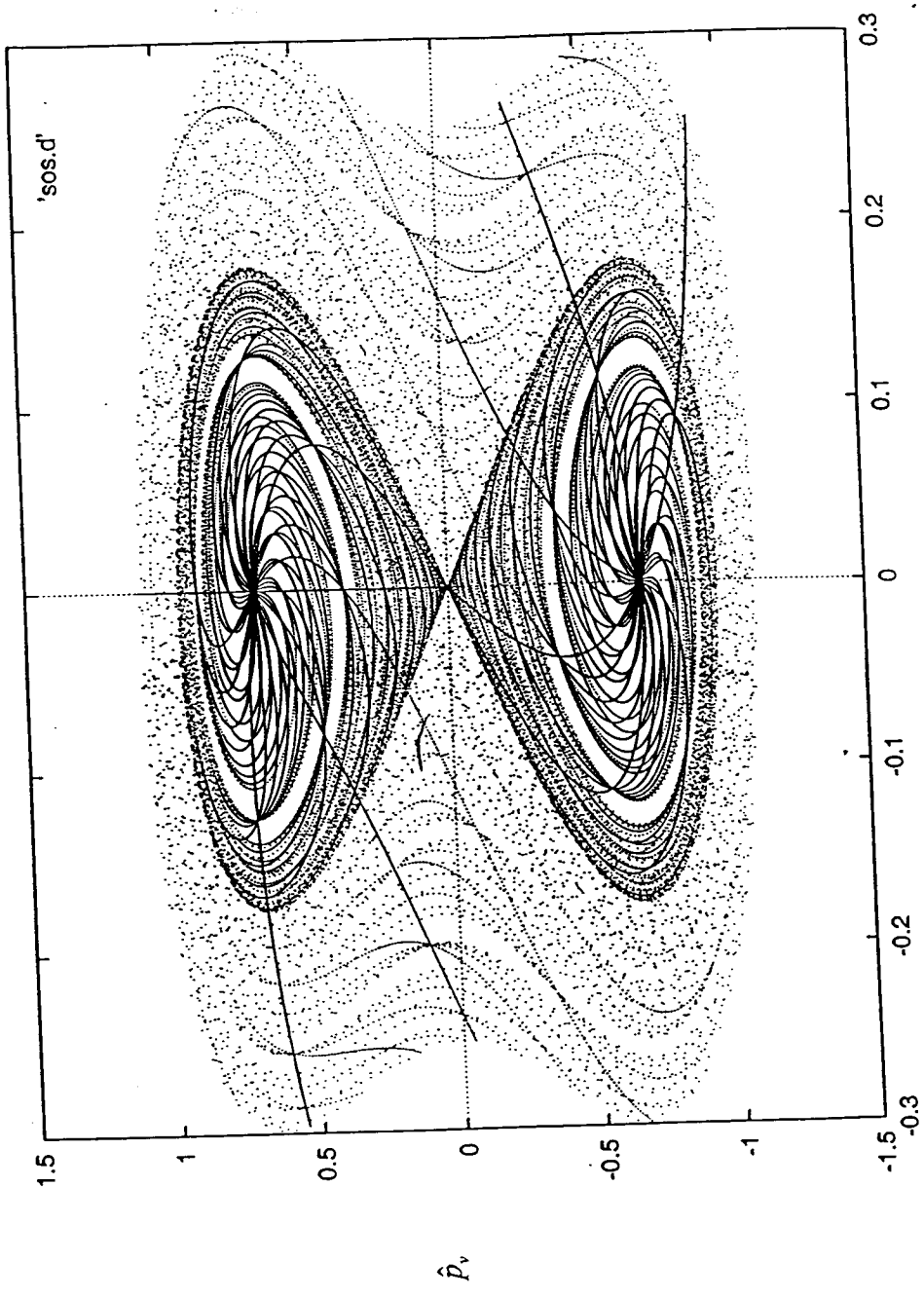

Figure 3.1. A "whorl" created by iterating a line of values of $\hat{p}_v$ between 0 and 1.1 on the $\hat{v}=0$ axis.

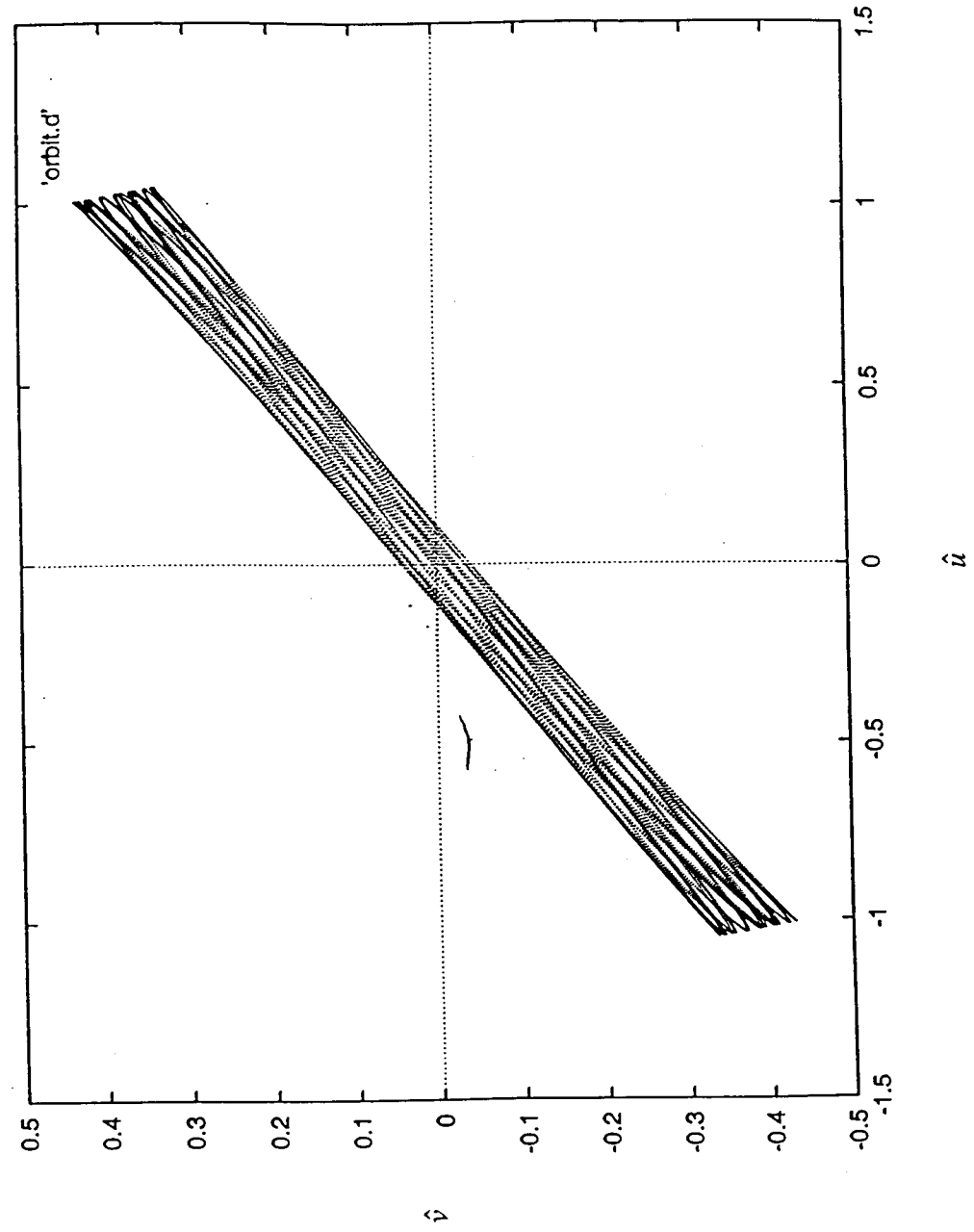

Figure 3.2. A regular motion orbit started at $\hat{v}=0, \hat{p}_v=0.6$.

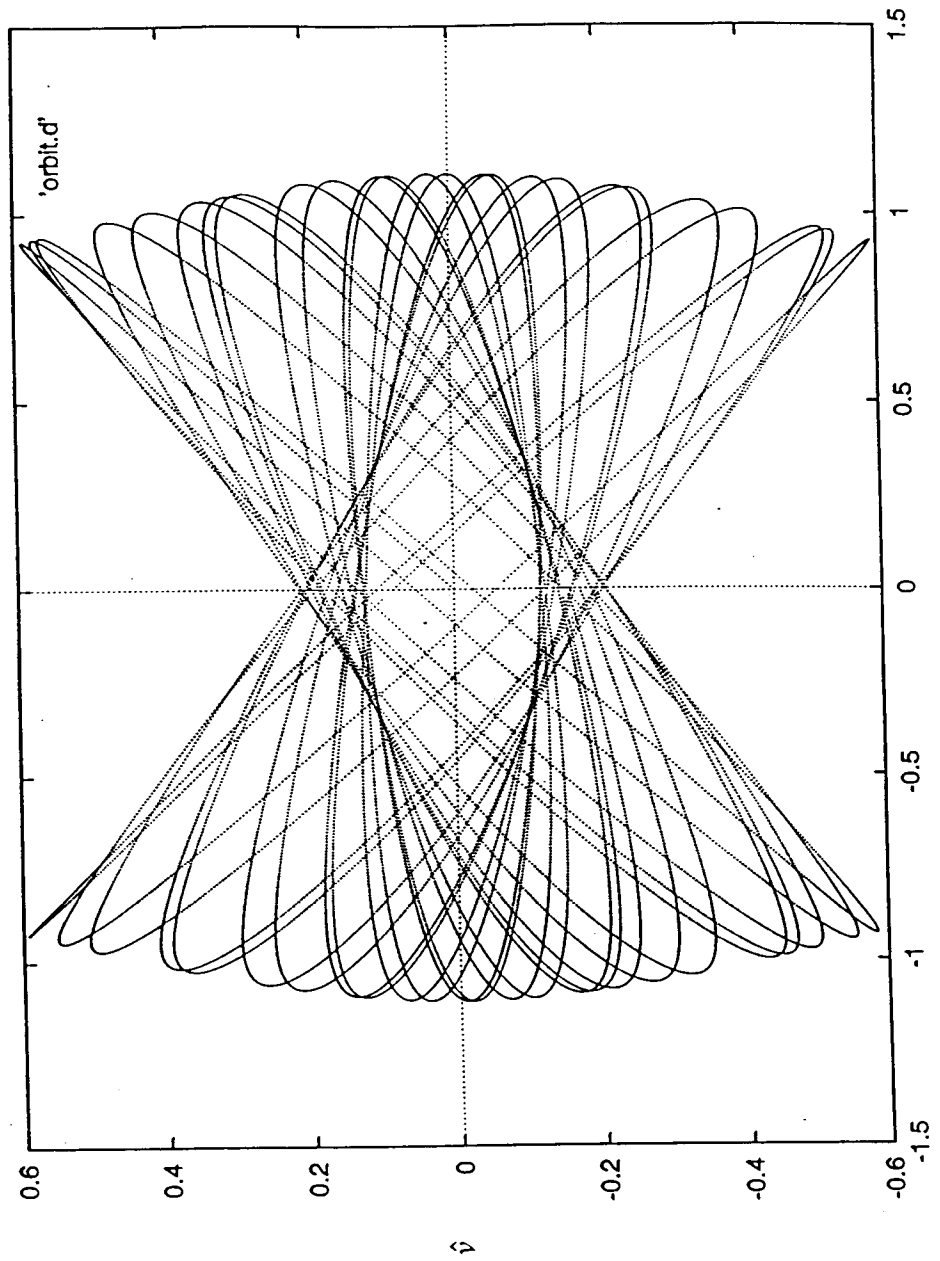

Figure 3.3. A regular motion orbit started at $\hat{v}=0, \hat{p}_v=1.0$.

Figure 3.4. A line segment on the $\hat{v}=0$ axis with values of $\hat{p}_v$ between 1.6 and 2 iterated. One sees these trajectories exit promptly roughly along the unstable manifold of the λ-point.

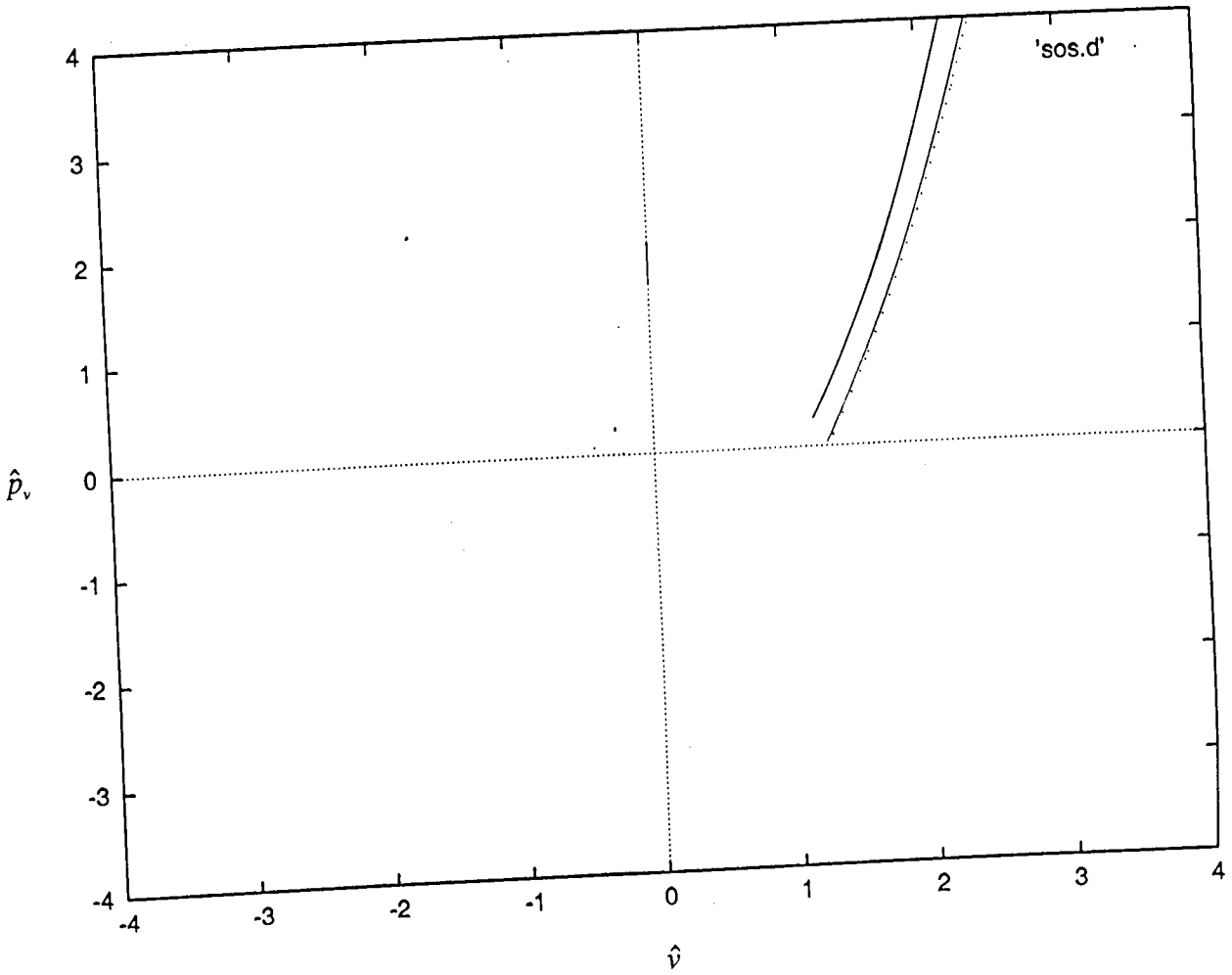

Figure 3.5. The surface of section created when a line segment of points on the $\hat{v}=0$ axis with values of $\hat{p}_v$ between 1.25 and 1.6. This segment was chosen as it corresponds closely to the region of the tangle. One can see that trajectories started in this region seem to trace a path alon: :he heteroclinic tangle.

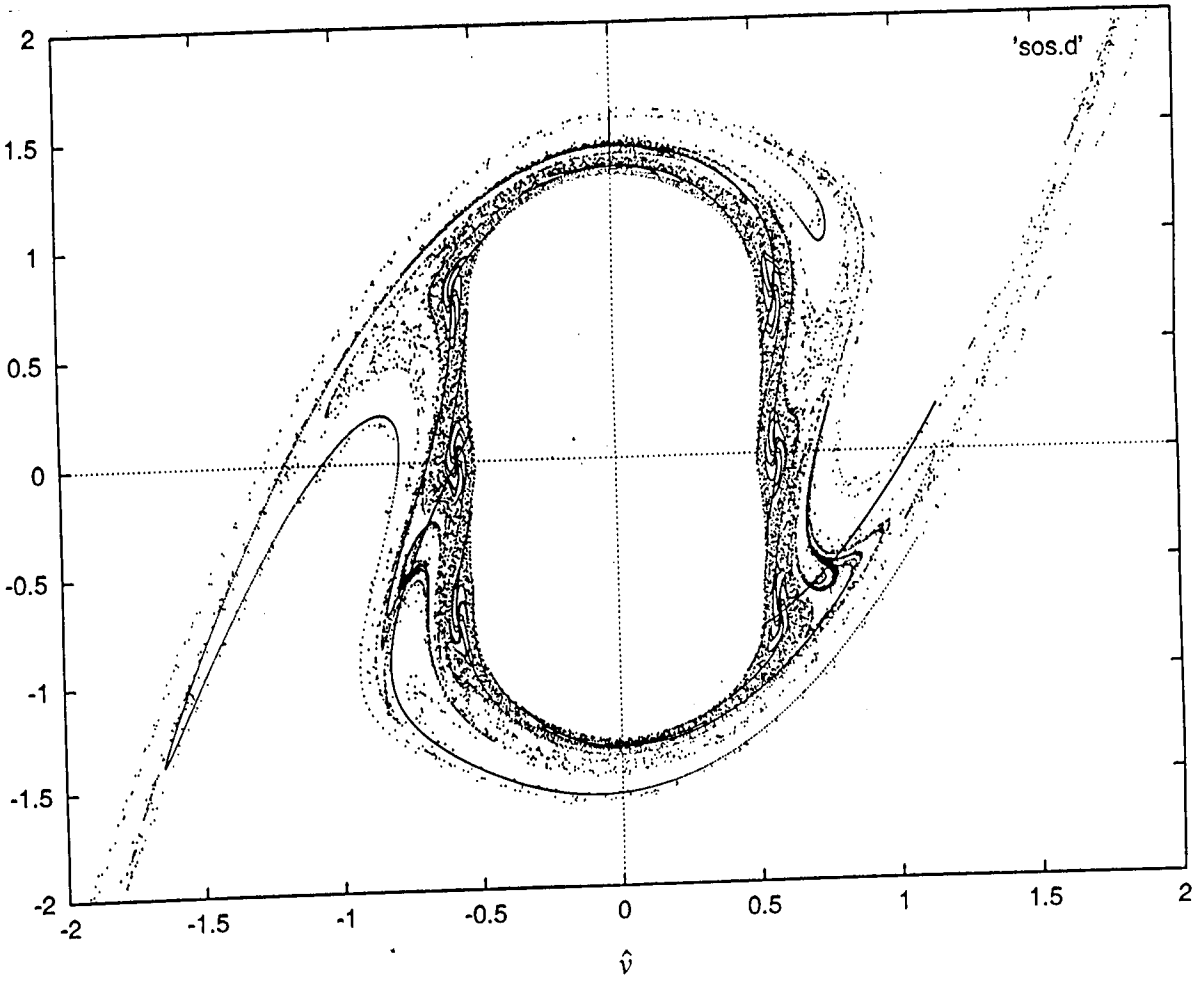

their initial momentum in the $\hat{y}$-direction, $\hat{p}$. By inspection of

Figure 3.6. Escape time as a function of $\hat{p}_v$ in the region of the tangle. Escape is defined as $|\hat{v}| \geq 2$. Negative escape time corresponds to negative $\hat{v}$ values, and positive escape time to positive $\hat{v}$ values.

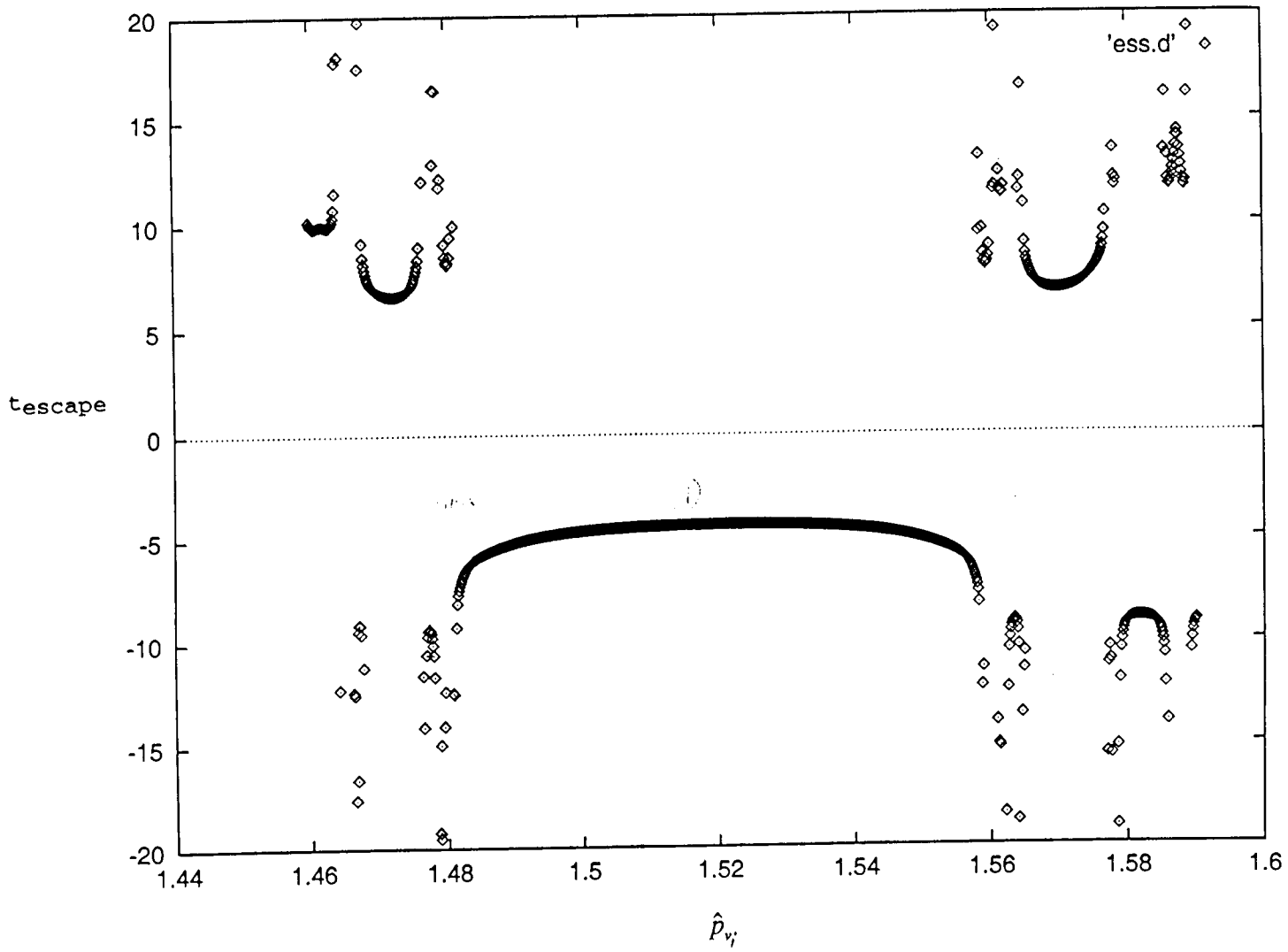

Figure 3.7. Blowing up a small region of Figure 3.3 reveals a similar pattern as that displayed in Figure 3.3 on the smaller scale of this graph.

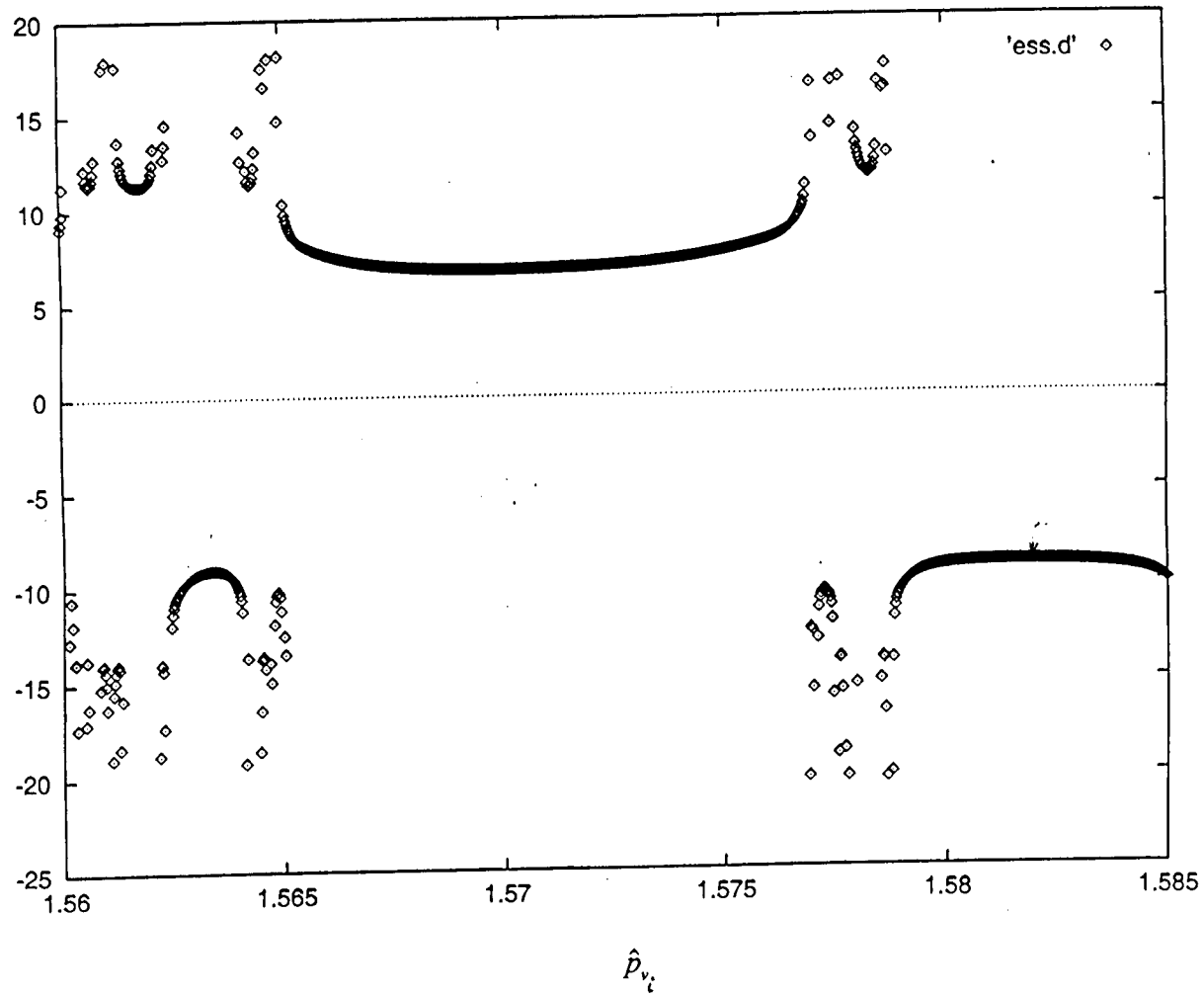

IV. Conclusion and Future of the Project

Through my study, I was able to take a system of practical interest and cast it in an elucidating form, in which I was able to control the amount of chaos in the system, by virtue of a parameterized coupling term. I identified the parameters of special interest to the system. These parameters were selected on the basis that they result in an equal mix of order and chaos, and a relatively easily determined heteroclinic tangle. Furthermore, I identified the short periodic orbits of the system and computed the heteroclinic tangle, which is the key t understanding a nonlinear system. After locating the tangle, it was possible for me to explain the motion in the bound region of the graph, the unbound region (outside of the tangle), and the chaotic behavior of trajectories begun in the region of the tangle. by studying these iterations of trajectories started at the atom, I was able to show that the heteroclinic tangle does indeed organize the behavior of the motion in phase space, by showing that the trajectories iterate so that they remain close to the tangle and follow its manifolds and tendrils. Finally, I have begun study of the escape times of trajectories in the system. From graphs I have generated it is evident that some sort of repeating pattern, structure within structure, exists. Further study and computation is necessary to verify that the function is, indeed, fractal.

The parameters which I have found to be of interest for this system have been sent to an experimental group in Amsterdam, rescaled with the magnetic field having a value of 0.1 T, making the values are appropriate and possible for experiment, so that the ionization of this system can be studied experimentally.

Appendix A:
Transforming the Hamiltonian

THEOREM 1: One way to obtain a canonical transformation is the following:

Suppose we have an original Hamiltonian, $h(p,x)$, such that:

$$\dot{x} = \frac{\partial h}{\partial p}$$

$$\dot{p} = -\frac{\partial h}{\partial x}$$

where x and p represent the original position and momentum. Let
P and X represent the new, transformed momentum and position.

1) Write any function of P, x:

$$W(P,x)$$

2) Set

$$p(P,x) = \frac{\partial W}{\partial x}$$

$$X(P,x) = \frac{\partial W}{\partial P}$$

3) Solve these equations either way to obtain

$$P(p,x)$$

$$X\big(P(p,x),x\big)$$

or,

$$x(P,X)$$

$$p\big(P,x(P,X)\big)$$

4) Take $H(P,X)$ as $h\big(p(P,X),x(P,X)\big)$. Then:

$$\frac{\partial P}{\partial t} = -\frac{\partial H}{\partial X}$$
$$\frac{\partial X}{\partial t} = \frac{\partial H}{\partial P}$$

and the form of Hamiltonian equations of motion are preserved, so the transformation is canonical.

Now we consider the case for which the change of coordinates depends on time. For our particular system, for instance, we will need to transform to a rotating coordinate system, which is obviously time dependent.

THEOREM 2: Suppose we have a set of "old" coordinates, (p,q), with the motion described by $p(t),q(t)$, and we wish to transform these coordinates into time-dependent ones, given by $P(p,q;t),Q(p,q;t)$, with the variable, t, being something that we impose on the system. We can use a generator

$$W(q,P;t)$$

such that

$$p(q,P;t) = \frac{\partial W(q,P;t)}{\partial q}$$
$$Q(q,P;t) = \frac{\partial W(q,P;t)}{\partial P}$$

The new Hamiltonian, H, equals the old Hamiltonian $+\frac{\partial W}{\partial t}$:

$$H = h\big(p(P,Q;t),q(P,Q;t)\big) + \frac{\partial W\big(q(P,Q;t),P;t\big)_{q,P}}{\partial t}$$

This transformation is canonical:

$$\frac{\partial P}{\partial t} = -\left(\frac{\partial H}{\partial Q}\right)_{P,t}$$
$$\frac{\partial Q}{\partial t} = \left(\frac{\partial H}{\partial P}\right)_{Q,t}$$

Now I can proceed to transform my coordinate system into a time-dependent one. This is prompted by Larmor's Theorem which states that the motion of a system of particles in a weak magnetic field is the motion in no field plus precession around the magnetic field axis. Thus, transforming to a coordinate frame that precesses at this Larmor frequency, ω_L, about the axis would simplify the motion.

Suppose we have a coordinate system (x',y',z'), as we do, and we wish to transform into a system which is rotating in one plane about the origin at a frequency ω_L. We will call the new system's coordinates (x,y,z). Since only the "plane of the orbit," the x'- y' plane is precessing, we need not worry about a transformation of the z' coordinate. Thus,

$$z = z'$$

Now, considering only the x-y plane, we wish to transform the original (x',y') coordinates into (x,y) coordinates as if the coordinate system were rotating with a frequency ω_L. Thus, at a time, t, the angle of rotation would be $\theta = \omega_L t$. Solving for x and y in terms of x' and y':

$$x = x'\cos(\omega_L t) + y'\sin(\omega_L t)$$
$$y = y'\cos(\omega_L t) - x'\sin(\omega_L t)$$

PROPOSITION: Now, in general, if we have any change of coordinates such that the new position variables depend only on the old position variables,

$$Q_1(q_1,q_2)$$
$$Q_2(q_1,q_2)$$

we can then choose new P's to get a canonical transformation by using the generator, W, such that:

$$W(q_1,q_2,P_1,P_2) = P_1Q_1(q_1,q_2) + P_2Q_2(q_1,q_2)$$

Then

$$Q_1 = \frac{\partial W}{\partial P_1} = Q_1(q_1, q_2)$$

$$Q_2 = \frac{\partial W}{\partial P_2} = Q_2(q_1, q_2)$$

and the new P's are, therefore, obtained from:

$$p_1 = \frac{\partial W}{\partial q_1} = P_1 \frac{\partial Q_1}{\partial q_1} + P_2 \frac{\partial Q_2}{\partial q_1}$$

$$p_2 = \frac{\partial W}{\partial q_2} = P_1 \frac{\partial Q_1}{\partial q_2} + P_2 \frac{\partial Q_2}{\partial q_2}$$

In order for a solution for P_1, P_2 to exist, then:

$$\left(\frac{\partial Q_1}{\partial q_1}\right)\left(\frac{\partial Q_2}{\partial q_2}\right) - \left(\frac{\partial Q_2}{\partial q_1}\right)\left(\frac{\partial Q_1}{\partial q_2}\right) \neq 0$$

Our transformation to a precessing coordinate system, outlined previously, is a special case of this type of situation, in which the new positions depend only on the old position variables and not the old momenta.

I begin the transformation by rewriting my original Hamiltonian (Eq. 1.1) in primed coordinates to remind us that it is the "old" frame, and converting from MKS to Gaussian-CGS units. Eq. 1.1 becomes:

$$H' = \frac{1}{2\mu}\left\{\left[p_x'^2 - \left(eBy'p_x'\right)\Big/c + \frac{\left(\frac{1}{4}e^2B^2y'^2\right)}{c^2}\right] + \left[p_y'^2 - \left(eBx'p_y'\right)\Big/c + \frac{\left(\frac{1}{4}e^2B^2x'^2\right)}{c^2}\right] + p_z'^2\right\} - \frac{Ze^2}{r} + eFz'$$

Referring to the previous proposition, my generator, W_L, will be:

$$W_L = p_x\left(x'\cos(\omega_L t) + y'\sin(\omega_L t)\right) + p_y\left(y'\cos(\omega_L t) - x'\sin(\omega_L t)\right)$$

The old momenta and new positions can be expressed as:

$$p_i' = \frac{\partial W_L}{\partial x_i'}$$

$$x_i = \frac{\partial W_L}{\partial p_i}$$

So,

$$p_x' = p_x\cos(\omega_L t) - p_y\sin(\omega_L t)$$
$$p_y' = p_x\sin(\omega_L t) + p_y\cos(\omega_L t)$$
$$p_z' = p_z$$

$$x = x'\cos(\omega_L t) + y'\sin(\omega_L t)$$
$$y = -x'\sin(\omega_L t) + y'\cos(\omega_L t)$$
$$z = z'$$

From Theorem 2, therefore, the new Hamiltonian, H, should equal:

$$H = H' + \frac{\partial W_L}{\partial t}$$

Finding expressions for $x'(x,y:t)$ and $y'(x,y:t)$ by adding and subtracting the simultaneous equations for x and y, plugging in for H' and simplifying, we get:

$$H' = \frac{p^2}{2\mu} + \frac{e^2B^2}{8\mu c^2}(x^2+y^2) + \frac{eB}{2\mu c}(xp_y - yp_x) + eFz - \frac{Ze^2}{r}$$

Now,

$$\frac{\partial W_L}{\partial t} = -\omega_L p_x x'\sin(\omega_L t) + \omega_L p_x y'\cos(\omega_L t) - \omega_L p_y x'\cos(\omega_L t) - \omega_L p_y y'\sin(\omega_L t)$$
$$\frac{\partial W_L}{\partial t} = \omega_L p_x y\sin^2(\omega_L t) + \omega_L p_x y\cos^2(\omega_L t) - \omega_L p_y x\cos^2(\omega_L t) - \omega_L p_y x\sin^2(\omega_L t)$$
$$= \omega_L(yp_x - xp_y) = \frac{eB}{2\mu c}(yp_x - xp_y)$$

Thus,

$$H = H' + \frac{\partial W_L}{\partial t} = \frac{p^2}{2\mu} + \frac{e^2 B^2}{8\mu c^2}\left(x^2 + y^2\right) + eFz - \frac{e^2}{r}$$

I have dropped the factor of Z in the last term since $Z=1$ for a hydrogen atom.

Next, I wish to transform to spherical polar coordinates, for which we, again, already know the relationship between old and new coordinates:

$$r = \left(x^2 + y^2 + z^2\right)^{\frac{1}{2}}$$

$$\theta = \tan^{-1}\left[\frac{\left(x^2 + y^2\right)^{\frac{1}{2}}}{z}\right]$$

$$\phi = \tan^{-1}\left(\frac{y}{x}\right)$$

So, now:

$$W = p_r r(x,y,z) + p_\theta \theta(x,y,z) + p_\phi \phi(x,y,z)$$

$$= p_r\left(x^2 + y^2 + z^2\right)^{\frac{1}{2}} + p_\theta \tan^{-1}\left[\frac{\left(x^2 + y^2\right)^{\frac{1}{2}}}{z}\right] + p_\phi \tan^{-1}\left(\frac{y}{x}\right)$$

Again, referring to our proposition:

$$F_i' = \frac{\partial W_L}{\partial x_i'}$$

So,

$$p^2 = \frac{p_r{}^2x^2}{r^2} + \frac{p_r{}^2y^2}{r^2} + \frac{p_r{}^2z^2}{r^2} + \frac{p_\theta{}^2x^2}{(x^2+y^2)z^2\left(1+\frac{x^2+y^2}{z^2}\right)^2} + \frac{p_\theta{}^2y^2}{(x^2+y^2)z^2\left(1+\frac{x^2+y^2}{z^2}\right)^2} + \frac{p_\theta{}^2(x+y}{z^4\left(1+\frac{x^2+}{z^2}\right.}$$

$$+ \frac{p_\phi{}^2}{x^2\left(1+\frac{y^2}{x^2}\right)^2} + \frac{p_\phi{}^2y^2}{x^4\left(1+\frac{y^2}{x^2}\right)^2}$$

$$= p_r{}^2 + \frac{p_\theta{}^2}{r^2} + \frac{p_\phi{}^2}{r^2\sin^2\theta}$$

Since, in this case, $\frac{\partial W}{\partial t} = 0, H = H'$, and so we get:

$$H = \frac{1}{2\mu}\left(p_r{}^2 + \frac{p_\theta{}^2}{r^2} + \frac{p_\phi{}^2}{r^2\sin^2\theta}\right) + \frac{e^2B^2}{8\mu c^2}\left(r^2\sin^2\theta\right) + eFr\cos\theta - \frac{e^2}{r}$$

Next, we move to semi-parabolic coordinates (u,v) for which :

$$u = \sqrt{r}\sqrt{1+\cos\theta}$$
$$v = \sqrt{r}\sqrt{1-\cos\theta}$$

There is not ϕ-dependence for these coordinates; thus, we are specifying cases for which p_ϕ=0.

Now,

$$W = p_u\left(\sqrt{r}\sqrt{1+\cos\theta}\right) + p_v\left(\sqrt{r}\sqrt{1-\cos\theta}\right)$$

$$p_r = \frac{\partial W}{\partial r} = \frac{1}{2\sqrt{r}}\sqrt{1+\cos\theta}\,p_u + \frac{1}{2\sqrt{r}}p_v\sqrt{1-\cos\theta}$$

$$p_\theta = \frac{\partial W}{\partial \theta} = -\frac{1}{2\sqrt{1+\cos\theta}}\sqrt{r}p_u\sin\theta + \frac{1}{2\sqrt{1-\cos\theta}}\sqrt{r}p_v\sin\theta$$

$$p_\phi = \frac{\partial W}{\partial \phi} = 0$$

So,

$$
\begin{aligned}
p^2 &= p_r^{\,2} + p_\theta^{\,2} + p_\phi^{\,2} \\
&= \left\{\left[\frac{p_u^{\,2}}{4r}(1+\cos\theta) + \frac{p_v^{\,2}}{4r}(1-\cos\theta) + \frac{1}{2}p_v p_u\left(\frac{1}{r}\right)\sqrt{1-\cos\theta}\sqrt{1+\cos\theta}\right]\right\} \\
&\quad + \left\{\frac{\left[\dfrac{p_u^{\,2} r\sin^2\theta}{4(1+\cos\theta)} + \dfrac{p_v^{\,2} r\sin^2\theta}{4(1-\cos\theta)} - \dfrac{p_u p_v r\sin^2\theta}{2\sqrt{1+\cos\theta}\sqrt{1-\cos\theta}}\right]}{r^2}\right\} \\
&= \frac{p_u^{\,2}}{4r}\left[\frac{(1+\cos\theta)^2 + \sin^2\theta}{1+\cos\theta}\right] + \frac{p_v^{\,2}}{4r}\left[\frac{(1-\cos\theta)^2 + \sin^2\theta}{1-\cos\theta}\right] + \frac{p_u p_v}{2r}\left[\frac{(1-\cos\theta)(1+\cos\theta) - \sin^2\theta}{\sqrt{1-\cos\theta}\sqrt{1+\cos\theta}}\right. \\
&= \frac{1}{2r}\left(p_u^{\,2} + p_v^{\,2}\right)
\end{aligned}
$$

Finally, using the relationships between (u,v) and (r,θ), and the above result for p2, we get as our transformed Hamiltonian:

$$
H = \frac{1}{2\mu}\left(\frac{p_u^{\,2} + p_v^{\,2}}{u^2+v^2}\right) + \frac{e^2B^2u^2v^2}{8\mu c^2} + eF\left(\frac{u^2 - v^2}{2}\right) - \frac{2e^2}{u^2+v^2}
$$

Appendix B:
Transforming the time variable

We need to change the time-dependence of our system so that our hamiltonian is no longer undefined at the origin of our coordinate system; as the term "u^2+v^2" appears in the denominator of the final Hamiltonian given in Appendix A, there is a singularity at the origin.

PROPOSITION: We introduce τ,

$$\tau = f(t)$$

such that:

$$\frac{dt}{d\tau} = g(p,q)$$

$$\frac{d(anything)}{dt} = \left(\frac{d\tau}{dt}\right)\frac{d(anything)}{d\tau}$$

Our revised Hamiltonian, H, is:

$$\mathrm{H} = \left[\frac{dt}{d\tau}(p,q)\right]\left[H(p,q) - E\right],$$

where E is the total energy.

PROOF:

$$\frac{dq}{dt} = \frac{\partial H}{\partial p_q}$$

$$\frac{dq}{d\tau} = \frac{dt}{d\tau}\frac{dq}{dt} = g(p,q)\left(\frac{\partial H}{\partial p_q}\right)$$

$$\frac{\partial \mathrm{H}}{\partial p_q} = \frac{\partial}{\partial p_q}\left[g(p,q)\left(H(p,q) - E\right)\right]$$

$$= \frac{\partial g(p,q)}{\partial p_q}\left[H(p,q) - E\right] + g(p,q)\frac{\partial\left(H(p,q) - E\right)}{\partial p_q}$$

$$= 0 + g(p,q)\left(\frac{\partial H}{\partial p_q}\right)$$

$$\therefore \mathrm{H} = g(p,q)(H - E)$$

For our particular system let $\frac{dt}{d\tau} = g = u^2 + v^2 = 2r$

Our H, then, becomes:

$$\mathrm{H} = \left(u^2+v^2\right)\left\{\left[\frac{1}{2\mu}\left(\frac{p_u{}^2 + p_v{}^2}{u^2+v^2}\right) + \frac{e^2B^2}{8\mu c^2}\left(u^2v^2\right) + eF\left(\frac{u^2-v^2}{2}\right) - \frac{2e^2}{u^2+v^2}\right] - E\right\}$$

$$= \frac{1}{2\mu}\left(p_u{}^2 + p_v{}^2\right) - E\left(u^2+v^2\right) + \frac{e^2B^2}{8\mu c^2}\left(u^4v^2 + u^2v^4\right) + eF\left(\frac{u^4-v^4}{2}\right) - 2e^2$$

Rewriting this in atomic units yields:

$$\mathrm{H} = \frac{1}{2}\left(p_u{}^2 + p_v{}^2\right) - E\left(u^2+v^2\right) + \frac{B^2}{8c^2}\left(u^4v^2 + u^2v^4\right) + F\left(\frac{u^4-v^4}{2}\right) - 2$$

Appendix C:
Rescaling to reduce number of parameters

We can now rescale the Hamiltonian so that $F=1$ and only B and E remain as explicit parameters. Now H=0, since it is simply equal to $g(u,v)(H-E)$ and $H-E=0$. So, to rescale:

$$p=\hat{p}F^{\alpha}$$
$$u=\hat{u}F^{\beta}$$
$$v=\hat{v}F^{\beta}$$
$$E=\hat{E}F^{\gamma}$$
$$B=\hat{B}F^{\sigma}$$

$$\hat{H}=0=F^{2\alpha}\frac{\left(\hat{p}_u{}^2+\hat{p}_v{}^2\right)}{2}-\hat{E}F^{\gamma}F^{2\beta}\left(\hat{u}^2+\hat{v}^2\right)+\frac{F^{2\sigma}\hat{B}^2}{8c^2}\left(\hat{u}^4\hat{v}^2+\hat{u}^2\hat{v}^4\right)F^{6\beta}+F^{1+4\beta}\left(\frac{\hat{u}^4-\hat{v}^4}{2}\right)-2$$

$$\hat{E}\left(\hat{u}^2+\hat{v}^2\right)=F^{-\gamma-2\beta}\left[F^{2\alpha}\frac{\left(\hat{p}_u{}^2+\hat{p}_v{}^2\right)}{2}+\frac{F^{2\sigma}\hat{B}^2}{8c^2}\left(\hat{u}^4\hat{v}^2+\hat{u}^2\hat{v}^4\right)F^{6\beta}+F^{1+4\beta}\left(\frac{\hat{u}^4-\hat{v}^4}{2}\right)-2\right]$$

All coefficients should equal zero to make F=1:

$$-\gamma-2\beta+2\alpha=0$$
$$-\gamma-2\beta+2\sigma+6\beta=0$$
$$-\gamma-2\beta+1+4\beta=0$$
$$-\gamma-2\beta=0$$

Solving these simultaneous equations yields:

$$\alpha=0$$
$$\beta=-\frac{1}{4}$$
$$\gamma=\frac{1}{2}$$
$$\sigma=\frac{3}{4}$$

So, finally,

$$\hat{H} = \frac{\left(\hat{p}_u{}^2 + \hat{p}_v{}^2\right)}{2} - \hat{E}\left(\hat{u}^2 + \hat{v}^2\right) + \frac{\hat{B}^2}{8c^2}\left(\hat{u}^4\hat{v}^2 + \hat{u}^2\hat{v}^4\right) + \frac{\left(\hat{u}^4 - \hat{v}^4\right)}{2} - 2$$

which is our final Hamiltonian, with the corresponding equations of motion:

$$\dot{\hat{p}}_u = -\left[-2\hat{E}\hat{u} + \frac{\hat{B}^2}{8c^2}\left(4\hat{u}^3\hat{v}^2 + 2\hat{u}\hat{v}^4\right) + 2\hat{u}^3\right]$$

$$\dot{\hat{p}}_v = -\left[-2\hat{E}\hat{v} + \frac{\hat{B}^2}{8c^2}\left(4\hat{u}^2\hat{v}^3 + 2\hat{u}^4\hat{v}\right) - 2\hat{v}^3\right]$$

$$\dot{\hat{u}} = \hat{p}_u$$

$$\dot{\hat{v}} = \hat{p}_v$$

It is these equations which are numerically integrated by the program in Appendix C to create my system's surfaces of section.

Bibliography

1. Balaz, N.L., Berry, M.V., Tabor, M., Voros, A., *Quantum Maps,* Annals of Physics: vol.122, 26-63. 1979.

2. Bleher, S., Brown, Reggie, Grebogi, C., Ott, E., *Fractal boundaries for exit in Hamiltonian dynamics,* Physical Review A. vol. 38, number2, 930-938. 1988.

3. Du, M.L., Delos, J.B., *Effect of closed classical orbits on quantum spectra: Ionization of atoms in a magnetic field. I. Physical picture and calculations,* Physical Review A, vol. 38, number 4, 1896-1911. 1988.

4. Delos, J.B., Gao, J. *Resonances and recurrences in the absorption spectrum of an atom in an electric field,* Physical Review A. vol. 49, number 2. 869-880. 1994.

5. Hilborn, R. C., Chaos and Nonlinear Dynamics. Oxford University Press, Oxford. pp. 317-363. 1994.